Design of Nanostructured Solar Cells Using Coupled Optical and Electrical Modeling

Michael G. Deceglie[†], *Vivian E. Ferry*[‡], *A. Paul Alivisatos*[‡], *and Harry A. Atwater**[,†]

[†] Thomas J. Watson Laboratories of Applied Physics, California Institute of Technology, Pasadena, California 91125, United States

[‡] Materials Science Division, Lawrence Berkeley National Laboratory, Berkeley, California 94720, United States

Abstract: Nanostructured light trapping has emerged as a promising route toward improved efficiency in solar cells. We use coupled optical and electrical modeling to guide optimization of such nanostructures. We study thin-film n-i-p a-Si:H devices and demonstrate that nanostructures can be tailored to minimize absorption in the doped a-Si:H, improving carrier collection efficiency. This suggests a method for device optimization in which optical design not only maximizes absorption, but also ensures resulting carriers are efficiently collected.

Keywords: Thin film solar cells, plasmon, nanophotonic, light trapping, simulation, device physics, silicon, photovoltaics

In order to maximize solar cell efficiency, it is necessary to optimize both the electrical device physics and the optical absorption of the device. Typically, these two problems are treated separately,

though compromises between them are frequently necessary.[1, 2] One route to realizing benefits to electrical and optical performance is to use the electrical advantages of thin absorbing layers in combination with light trapping structures to increase optical absorption within the active layer. The electrical benefits of thin absorbing layers vary for different materials systems.[2-5] For collection-limited semiconductors, thin absorbing layers reduce the need for long diffusion lengths. For hydrogenated amorphous Si (a-Si:H) cells, decreased thickness can lead to improved stability and increased open circuit voltages (V_{oc}).[4, 5] In addition, thin active regions offer the advantage of decreased cell manufacturing time and cost of raw materials, and enable large scale deployment of scarce materials.[5, 6] However, efficient light trapping is critical to realizing these benefits of thin devices.

Conventional a-Si:H solar cells utilize roughened textures, which may consist of textured transparent conducting oxides, plastics, or metals, to trap light within the semiconductor.[7, 8] In recent years, the deliberate design of nanostructures to guide light into thin semiconductor regions has emerged as an active area of research, with a wide variety of proposed plasmonic and nanophotonic structures.[2, 4, 6, 9-19] Such nanostructures offer the ability to control light absorption within a device, and many studies take advantage of theoretical optical analysis to model absorption in these devices and optimize the light trapping structures.[9] To date, most theoretical studies of light trapping account only for optical effects, but modeling both the electronics and optics of advanced photovoltaic devices is preferable in order to account for carrier recombination and realistically predict device performance.[20, 21]

In this design study, we use optical simulations coupled with device physics simulations to enable the simultaneous optimization of both the device physics and optics of nanostructured n-i-p a-Si:H solar cells. By understanding the effects of enhanced absorption on device physics, we demonstrate that, in addition to improving light absorption, careful treatment of the device optics offers a new path toward the optimization of the electrical device performance.

The integration of nanostructures in solar cells significantly changes the mechanism of light absorption. In bulk semiconductor, light is absorbed exponentially from front to back. In a thin film with a back reflector, incompletely absorbed light can reflect off each interface several times, making multiple passes through the semiconductor as in a Fabry-Perot cavity.[22] When nanostructures are introduced, however, the absorption in the film will depend on many effects such as scattering, localized modes, and guided modes, which significantly modify both the magnitude and the location of absorption within the thickness of the device.[12, 14, 19, 23-26]

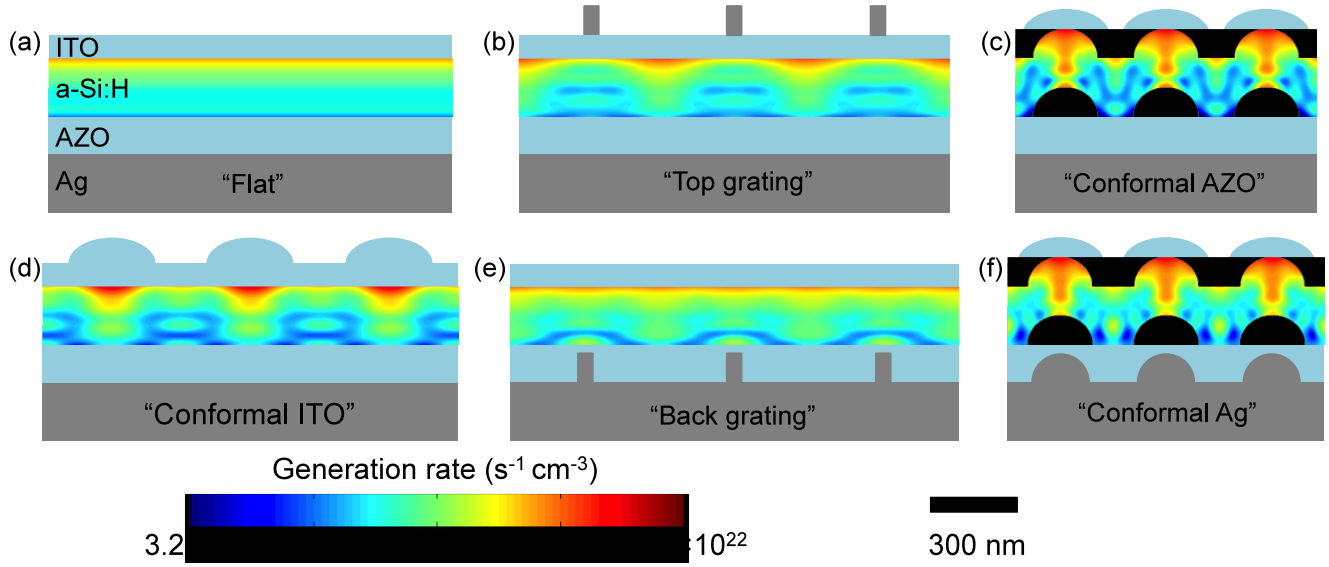

Figure 1. Solar cell structures studied here (drawn to scale) with 200 nm thick a-Si:H. The carrier generation rates calculated from FDTD simulations of AM1.5G illumination are plotted in the a-Si:H regions on logarithmic scale. The structures are based on an 80 nm thick indium doped tin oxide (ITO) layer, a variable thickness n-i-p a-Si:H layer (200 nm pictured), a 130 nm aluminum doped zinc oxide (AZO) layer, and a 200 nm thick Ag back reflector. The Ag ridges in (b) and (e) are 100 nm tall and 50nm wide. The curved Ag structures in (f) are semi-circles with a radius of 100nm. All other curved surfaces are semi-ellipses with horizontal major axes. The curved ITO structures in (c), (d), and (f) have a major radius of 150 nm and a minor radius of 80 nm. The curved AZO and a-Si:H structures have a major radius of 110 nm and a minor radius of 100nm. The feature pitch for each structure is given in Table 1.

Figure 1 shows optical generation rates calculated using finite-difference time-domain (FDTD) simulations for a variety of light trapping structures. The structures are based on (from top to bottom) an

80 nm thick indium doped tin oxide (ITO) layer which also acts as an anti-reflection coating, a variable thickness n-i-p a-Si:H layer, a 130 nm aluminum doped zinc oxide (AZO) layer, and a 200 nm thick Ag back reflector. The AZO layer is commonly employed in n-i-p a-Si:H devices both to block diffusion of the Ag into the a-Si:H during growth and to decrease optical losses associated with coupling to surface plasmon polariton modes.[26] AZO, instead of ITO, is commonly used for this purpose because ITO is not compatible with the plasma enhanced vapor deposition used to deposit the a-Si:H layers.[27] Both AZO and ITO are commonly used for the top transparent contact,[27] but in this work we choose ITO to more closely represent previously reported structures that are similar to those studied here.[4, 10] Except where otherwise noted, both optical and electrical simulations were done in two dimensions; the corresponding implied three-dimensional structures would be extended in the third dimension to make grating-like structures. Both polarizations of incident light were simulated, and the generation rates averaged to resemble an unpolarized source. The carrier generation rates calculated from the FDTD results were taken as input into finite element device physics calculations in order to understand the full optical and electrical performance of the device in a unified manner. In particular, we study how different generation rate profiles, such as those pictured in Figure 1, which can depart significantly from the profiles obtained with Beer-Lambert absorption or thin-film interference,[22] affect the electrical device performance.

We explore several different geometries of light trapping structures. In the first two designs, the a-Si:H is flat, and a plasmonic ridge is included either on top of the ITO (Figure 1b, "top grating") or built into the back contact (Figure 1e, "back grating"). In the top grating geometry, the scattering cross section of the ridge, which may be several times larger than its geometrical cross section, couples light preferentially into the semiconductor film. This both increases the path length of the incident light and may couple to the waveguide modes of the structure. In the back grating geometry, the ridge is built

directly into the back contact. In this case, light on the blue side of the spectrum will be absorbed by its standard process, while incompletely absorbed red light will scatter from the nanostructure and couple into waveguide modes of the cell. In the third geometry (Figure 1d, "conformal ITO") we directly structure the ITO while maintaining a flat a-Si:H layer.[9] In the last two geometries, we study cells with both front and back texturing, as would be realized in experimental devices with conformal deposition.[4, 9] In the case shown in Figure 1f ("conformal Ag"), there is both a plasmonic Ag structure on the back interface and a conformal AZO structure coated over the Ag. In the geometry shown in Figure 1c ("conformal AZO"), the Ag layer is a flat mirror but the AZO structure is maintained. As shown in Figure 1, the different nanostructures result in different generation rate profiles.

The different light trapping geometries described here utilize not just plasmonic nanostructures, but also structured semiconductors and dielectrics. For the designs including nanostructured metals, there are several distinct mechanisms that may contribute to plasmonic light trapping.[6] Plasmonic nanostructures exhibit large scattering cross sections, which may be several times their geometrical cross section. In the cases described here, with metal nanostructures on the back contact, the coupled metal nanoparticle / metal film system acts as a plasmonic scatterer for incident sunlight, redirecting light absorption into the cell and potentially coupling into waveguide modes of the device. The metallic nanostructures could also increase absorption locally due to their enhanced local electric field, but the AZO layer here is 130 nm thick, making a local field enhancement unlikely. The waveguide modes of the devices could be either photonic guided modes or surface plasmon polariton (SPP) modes supported on the metal interface; however the presence of the AZO decreases coupling to the SPP modes, as has been discussed elsewhere.[9, 26]

To enable straightforward comparison, the conformal geometries were chosen such that the total volume of a-Si:H is the same as a flat-absorber cell of the same a-Si:H layer thickness. Similarly, the

doped regions are thinned over the curved surfaces of the conformal AZO and Ag structures (Figure 1c and 1f) to maintain the volume ratio of doped to undoped material. We define the parameter d to be the thickness of each doped region in a corresponding flat-absorber cell. For example, in a conformal cell of d = 20 nm, the doped regions are 20 nm thick on the flat surfaces and 13.3 nm thick over the curved surfaces.

The optical generation rate was calculated at each wavelength in the solar spectrum, with 10 nm spectral resolution, where a-Si:H is optically active (350 – 800 nm). The generation rate at each incident wavelength, $G_{opt}(\lambda)$, can be calculated directly from FDTD using

$$G_{opt}(\lambda) = \frac{\varepsilon'' |E|^2}{2\hbar}$$

where ε'' is the imaginary part of the permittivity and E is the (optical) electric field. While losses in all of the materials are included in the simulation, we calculated the generation rate in the a-Si:H by isolating only the data in the region containing a-Si:H after the simulation is complete. Likewise, we can calculate parasitic losses by integrating over the region of the simulation containing the other materials. These sources of parasitic absorption in layers other than the a-Si:H are non-negligible, as we describe in the Supporting Information. We then weighted $G_{opt}(\lambda)$ by the AM1.5G spectrum to get the solar spectrum weighted (white-light) G_{opt}. We simulated each structure under both transverse magnetic and transverse electric polarizations, and average the results for input to the device simulation. The complex refractive index for ITO, AZO, and a-Si:H were taken from previously measured data,[4] and Ag was modeled using a Lorentz-Drude fit to data from Palik[28], following the method of Rakic et al.[29] The FDTD simulations were carried out with a commercial FDTD software package.[30]

These white-light carrier generation profiles in the a-Si:H were interpolated onto a finite element mesh for electrical device simulation with a technology computer-aided-design software package.[31] Only the n-i-p a-Si:H region was modeled electrically, and ohmic contacts were assumed. We note that

the assumption of ohmic contacts implies infinite surface recombination velocity at the contacts.[32] The electrical parameters for a-Si:H used in this study were taken from Schropp and Zeman[27], with the exceptions that the mobility band-gap in all layers was assumed to be constant at 1.78 eV for simplicity and the peak dangling bond trap concentration in the intrinsic region was set to 2×10^{17} cm^{-3} eV^{-1} to reproduce the experimental observation of decreasing V_{oc} with increasing a-Si:H thickness.[4] A full list of the electrical parameters used in this study is provided in the Supporting Information. The full electrostatics and statistics of the band tail and dangling bond trap distributions in a-Si:H were explicitly included.

White-light current-voltage (J-V) curves were calculated by varying the voltage boundary conditions at the contacts and numerically solving the electrostatic and carrier transport equations[32] on a finite element mesh for each voltage. From these J-V curves, we calculated standard solar cell performance parameters: short circuit current density (J_{sc}), open circuit voltage (V_{oc}), fill factor (FF), and conversion efficiency.[33] We also calculated a white-light "electrical internal quantum efficiency" (EIQE) of the a-Si:H from the ratio of J_{sc} to K. K is defined as the generation current density, and is obtained from the spatially integrated generation rate (after interpolation to the finite element device simulation grid) over the a-Si:H layer, assuming unity carrier collection. Note that this definition of EIQE, used throughout this study, varies from the internal quantum efficiency which is commonly experimentally measured in that absorption in layers other than the a-Si:H is neglected. The quantity EIQE is useful in that it allows us to isolate the electrical behavior of the device from optical effects. In addition, we calculated the intrinsic region generation current density by integrating over only the intrinsic a-Si:H region, and denote this quantity as K_i.

We also studied the spectral response of the devices by taking the generation rate profiles for each incident wavelength as input into the device physics simulations. For the purposes of the electrical

simulations, the illumination power at each wavelength was set to 10 mW cm^{-2}. The resulting electrical currents for each wavelength were then calculated for the device at short circuit and weighted by the AM1.5G solar spectrum. This weighting makes the choice of illumination intensity for the purposes of the simulations themselves arbitrary, so long as it does not alter the device physics with respect to the white-light case. To verify this, we integrated the solar spectrum weighted currents over the wavelength range of interest (350 – 800 nm), and found that the results matched the calculated white-light J_{sc} to within 0.2%. This indicates that the device physics affecting charge collection are not significantly altered with the choice of 10 mw cm^{-2} as the illumination power at each wavelength for the spectral response simulations. As in the white-light simulations, K and K_i were also calculated for each wavelength.

For each of the structures shown in Figure 1, we simulated a range of nanostructure periodicities. The optimal pitch depends on the scattering and absorption cross sections of the features, the strength of their coupling to the waveguide modes, and the constructive and destructive interference of the waveguide modes. Therefore, the optimal pitch varies depending on the light trapping geometry. Table 1 summarizes the electrical and optical performance calculated for each structure at its optimal pitch under white-light illumination. From these results it is apparent that designing light trapping structures to maximize the absorption current density, K, in the semiconductor is the dominant factor in obtaining optimized efficiency in this system. However, it is not clear from these results whether the change observed in V_{oc} is due to changing photocurrent or to effects of non-standard spatial distributions of carrier generation.

To address this, we also calculated the electrical performance of each structure with its J_{sc} matched to that of the flat control structure. This was achieved by scaling the generation profile down by a multiplicative factor prior to inputting it into the device physics simulation. The results of these

simulations are given in Table 2. From them, we conclude that departures from a flat thin-film interference absorption pattern[22] do not significantly change the relationship between the electrical parameters themselves. The dominant effect of the light trapping structures is therefore to vary J_{sc}. The V_{oc} and FF vary only in as much as they depend on J_{sc}. We do note however that the different profiles, when proportionally scaled, display different white-light EIQEs at short circuit. This indicates that some carrier generation profiles are electrically collected more efficiently than others at short circuit.

Table 1. Electrical and Optical Performance Parameters for 200 nm Thick a-Si:H Solar Cells with d = 20 nm Extracted from Simulations for a Flat Control and the Optimized Pitch of Each Structure Shown in Figure 1.

structure	pitch (nm)	K (mA cm^{-2})	efficiency	J_{sc}(mA cm^{-2})	V_{oc} (V)	FF
flat	-	9.22	4.94	6.48	0.953	80.0
top grating	500	9.38	5.07	6.64	0.954	80.0
back grating	520	10.28	5.52	7.21	0.957	80.1
conformal ITO	480	9.70	5.14	6.72	0.955	80.1
conformal AZO	340	11.85	6.86	8.75	0.963	81.4
conformal Ag	360	12.28	7.25	9.25	0.965	81.3

Table 2. Electrical and Optical Performance Parameters for the Devices in Table 1 with the Generation Rate (G_{opt}) Scaled to Match the Short Circuit Current Density of the Flat Control.

structure	pitch (nm)	K (mA cm^{-2})	efficiency	J_{sc}(mA cm^{-2})	V_{oc} (V)	FF
flat	-	9.22	4.94	6.48	0.953	80.0
top grating	500	9.16	4.94	6.48	0.953	80.0
back grating	520	9.19	4.94	6.48	0.953	80.0
conformal ITO	480	9.36	4.94	6.48	0.953	80.1
conformal AZO	340	8.78	5.00	6.48	0.952	81.1
conformal Ag	360	8.60	5.00	6.48	0.952	81.1

This effect is quantified in Figure 2, which shows that the short circuit EIQE correlates with the fraction of absorption current in the intrinsic region. These calculations assume doped regions of d = 20 nm. This correlation is understood by noting that the doped regions have much higher densities of dangling bond trap states than the intrinsic a-Si:H, and thus electron hole pairs generated in the doped regions are subject to higher Shockley-Read-Hall recombination rates making them less likely to be collected as photocurrent.[27] The correlation in Figure 2 indicates the importance of light trapping structures designed to target enhancements in the intrinsic region of the cell, thus avoiding parasitic absorption losses in the doped regions.

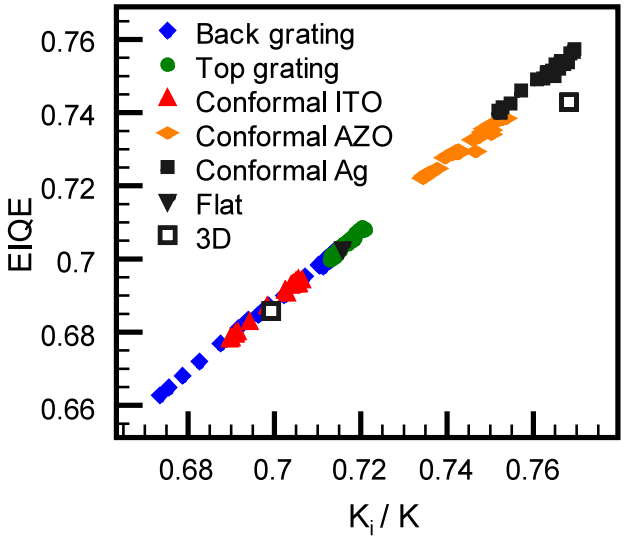

Figure 2. White-light electrical internal quantum efficiency at short circuit plotted against the ratio of absorption current density generated in the intrinsic region (K_i) to the total absorption current density (K) generated in the a-Si:H for the structures shown in Figure 1, along with two 3D structures, with d = 20 and varying pitch. We observe a correlation across all structures, indicating the importance of avoiding parasitic absorption in the doped regions of a-Si:H solar cells.

Though this study focuses primarily on 2D simulations to take advantage of reduced computational demand, we include the results of two 3D simulations in Figure 2 in order to demonstrate that our methods and observations extend to 3D light trapping structures and devices. The schematics and calculated J-V curves for these two structures are given in Figure 3. In both cases, the optical and electrical simulations were carried out for the full 3D device structure. Both devices have d = 20 nm.

The device pictured in Figure 3a corresponds to the point at $K_i/K = 0.77$ in Figure 2 and is based on the "conformal Ag" structure, but the curved surfaces are 3D semi-ellipsoids. In this case, the doped regions are thinned to 10.5 nm over the curved surfaces. We calculated a white-light conversion efficiency of 7.37% for this structure, with $J_{sc} = 9.36$ mA cm^{-2}, $V_{oc} = 0.968$ V, and $FF = 81.3$. The device pictured in Figure 3b corresponds to the point at $K_i/K = 0.7$ in Figure 2 and includes only the hemispherical structuring on the Ag back reflector, all other layers, including the a-Si:H, are flat. For this device, we calculated a white-light conversion efficiency of 5.04%, with $J_{sc} = 6.59$ mA cm^{-2}, $V_{oc} = 0.956$ V, and $FF = 80.1$. Both devices are based on a square array of the light trapping structures with 300 nm pitch.

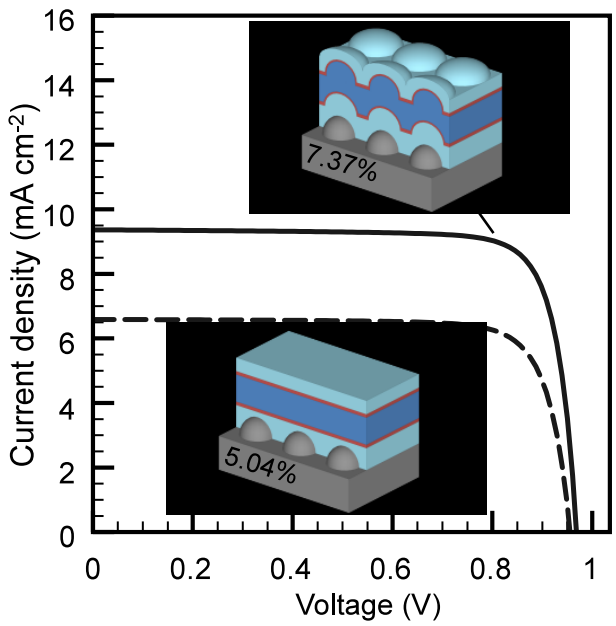

Figure 3. Current-voltage curves and one-sun conversion efficiencies calculated with full 3D optical and electrical simulations. The schematics are drawn to scale and have the same color scheme as in Figure 1, but with intrinsic a-Si:H indicated as dark blue and doped a-Si:H indicated as red. The upper layers are cut away in the schematics to reveal the underlying structure of the Ag layer.

Our model predicts that nanostructuring of the a-Si:H layer itself does not degrade V_{oc}, but rather that V_{oc} is improved due to increased photocurrent (Tables 1 and 2). This result agrees with experimental reports that indicate high V_{oc} can be maintained or improved in nanostructured a-Si:H solar cells.[10, 19] However, there are several possible effects that could lead to a reduction of V_{oc} in

nanostructured solar cells. First, increased surface area can result in increased surface recombination. In the structures studied here, the doped regions do not contribute to useful photocurrent (Figure 2), and thus an increase in the doped region / contact surface area does not negatively affect V_{oc}. Another potential source of V_{oc} degradation is the increased junction area of the device. However, this prediction is not applicable to n-i-p a-Si:H solar cells since trap-mediated recombination in the bulk, and not the forward bias current injected across the junction of an ideal diode, is the primary mechanism competing with photocurrent collection.[34-36] Finally, deposition on textured substrates can lead to degradation in the material quality of the active layers in thin-film Si solar cells, and in turn a reduction of the V_{oc}.[37, 38] We note that our model allows for the inclusion of such effects. This could be accomplished, for example, by changing the bulk trap densities in the a-Si:H regions as the geometry becomes rougher, or incorporating localized regions of high trap density near particular geometric features. In these cases, it would be beneficial to use empirical data from a specific process protocol as the basis for the simulation parameters.

Since the performance of the devices studied here is dominated by photocurrent increases due to light trapping, it is critical to understand the factors underlying efficient carrier collection. We note the significance of the observation that the correlation in Figure 2 holds for all the structures studied, including conformal ones. This, in combination with the results in Table 2, demonstrates that parasitic absorption in doped regions dominates any other performance variations arising from electrical collection, even under bias, of non-standard absorption profiles.

The two structures with conformal a-Si:H layers exhibit higher white-light EIQE than any of the flat devices (Figure 2). This is due to decreased parasitic absorption of the blue part of the spectrum in the front p-doped layer, which is thinned over the curved surface. We note that similar geometries have been shown experimentally to exhibit enhanced external quantum efficiency at short wavelengths

attributed to improved anti-reflection performance and resonant absorption in the semiconductor nanostructures.[4, 39] However, we are comparing values of EIQE which isolate the internal electrical performance of the structure from optical effects such as reflection and resonant absorption.

Among the conformal structures, the conformal Ag structure, which includes plasmonic Ag structures in the back contact, consistently demonstrates higher EIQE than the conformal AZO structure, which has a flat Ag surface. Thus there is a two-fold advantage for the conformal Ag structure, which includes plasmonic structures, as compared to the conformal AZO structure; it increases the overall light absorbed in the semiconductor, while simultaneously ensuring that the resulting charge carriers are more efficiently collected (Table 1).

Careful examination of the spectral response of the two designs reveals the source of this advantage for the conformal Ag structure. Figure 4a shows that, for the optimal pitches of the conformal Ag and AZO structures, the increase in optical absorption and corresponding electrical current of the conformal Ag structure result from an enhancement near an incident wavelength of 650 nm. Figure 4b,c show the details of the generation rate profile of 650 nm light for each structure, indicating that the increase in absorption in the conformal Ag case is concentrated in the intrinsic region. The result is that carriers generated from 650 nm light are collected at short circuit with an EIQE of 0.84 for the conformal Ag structure, as opposed to 0.79 for the conformal AZO structure.

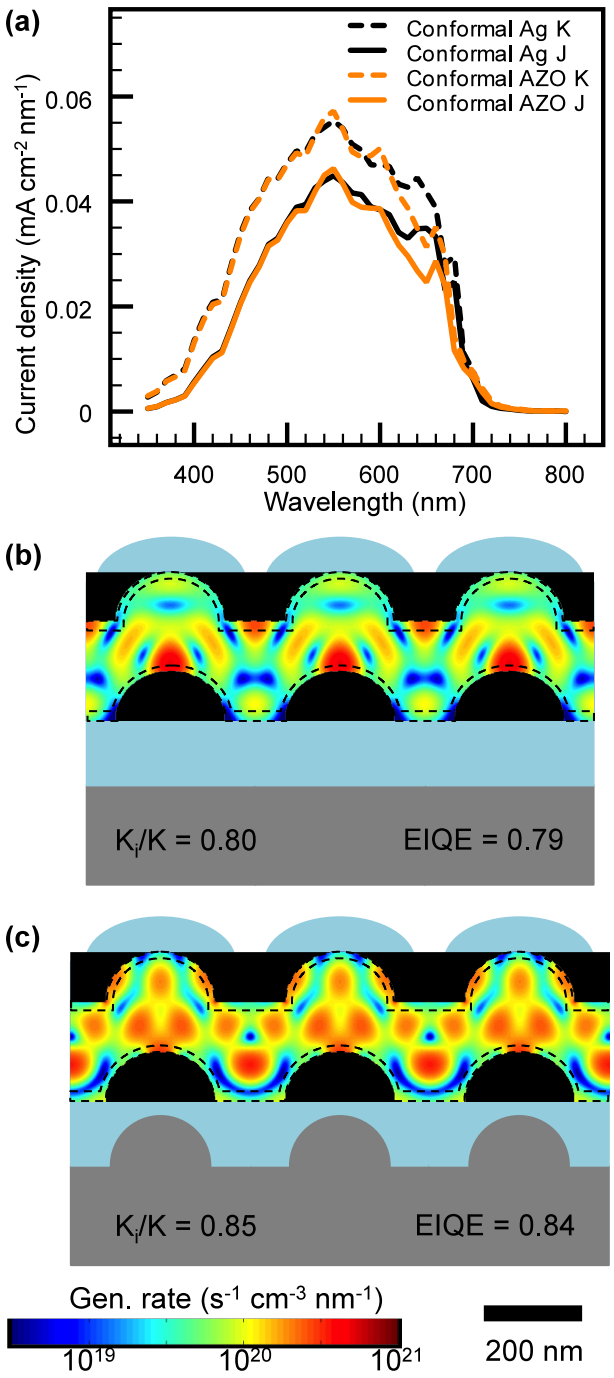

Figure 4. (a) Optical and electrical spectral response calculated for the conformal Ag (360 nm pitch) and conformal AZO (340 nm pitch) structures with 200 nm thick a-Si:H layers and d = 20 nm, for the AM1.5G spectrum. (b, c) The generation rate from 650 nm light calculated for the conformal AZO (b), and conformal Ag (c) structures plotted on a logarithmic scale, showing the performance enhancement in the conformal Ag structure comes from an optical mode with an improved K_i/K ratio for 650 nm incident light resulting in improved EIQE at that wavelength. The dashed lines indicate the edges of the doped a-Si:H regions.

This example demonstrates the two-fold advantage of including a nanostructured Ag back reflector in the conformal design; it is able to collect more light (Figure 4a) and simultaneously use advantageous optical design to reduce the portion of generated current lost to parasitic absorption in the doped regions (Figure 4b,c). We estimate that the improvement from EIQE accounts for approximately one quarter of the relative efficiency improvement between the two structures (Table 1), with the remainder coming from the optical absorption enhancement. We make this estimate by multiplying the generated current density K in the conformal Ag device by the EIQE of the conformal AZO structure to estimate the J_{sc}; no adjustment is made to the FF or V_{oc}, as these corrections would be small.

This result suggests a novel route toward optical solar cell design, in which light trapping structures are designed to take advantage of electrical device physics effects. In particular, light trapping structures for thin-film devices should target enhancement in optical modes that result in efficiently collected carrier generation profiles. In the example considered here, where minimization of parasitic absorption is the dominant effect, a similar benefit to both the EIQE and overall absorption current could be realized without light trapping by thinning the doped regions or increasing the overall thickness of the device.

The effects of such an optimization on the J-V curve of a flat device are shown in Figure 5b, along with a thinner un-optimized flat cell (Figure 5a) and a comparable conformal Ag cell (Figure 5c). The devices in Figure 5a and c are comparable in that they utilize the same volume of a-Si:H and the volume ratio of doped to intrinsic a-Si:H is the same. For the optimized flat device (Figure 5b), we see the advantage of incorporating thinner doped regions in a thicker overall device structure; the overall absorption current density is increased from 9.40 mA cm^{-2} to 11.66 mA cm^{-2} and the short circuit EIQE is increased from 0.70 to 0.84 compared to the structure in Figure 5a. However, in contrast to the case

where light trapping design is used to target high absorption and improved EIQE (Figure 5c, V_{oc} = 0.965, FF = 81.3), the optimized flat device suffers degradation of V_{oc} (0.939 V) and FF (72.3).

The benefit of coupled optical and electrical optimization is apparent in the result that, in the limiting case of perfectly flat layers, the maximized efficiency of 6.58% remains less than the efficiency of 7.25%, which can be achieved in a thinner device with conformal light trapping structures and thicker doped regions (Figure 5c). This thinner design with conformal light trapping structures increases absorption and EIQE without degradation of *Voc* or *FF* (Table 1). It also has the advantages of reduced processing costs of Si deposition, reduced light induced degradation, and decreased vulnerability to non-uniformities in the thicker doped regions.[4, 5] All these benefits are realized while achieving a higher efficiency than an optimized flat cell.

The efficiency of the conformal Ag design is maximized by increasing the a-Si:H thickness to 290 nm and thinning the doped regions to d = 10 nm (Figure 5d). The optimized feature pitch for this structure is 390 nm. This design yields an efficiency of 8.32% with J_{sc} = 11.29 mA cm^{-2}, V_{oc} = 0.955 V, FF = 77.2, and white-light EIQE = 0.87. We note that the a-Si:H is 70 nm thinner than in the optimized flat device (Figure 5a), resulting in improved V_{oc} and FF. The fact that it also exhibits higher J_{sc} and EIQE than the optimized flat device, despite an increased ratio of doped to undoped a-Si:H, highlights the power of coupled optical and electrical optimization.

Though we demonstrate that our methods extend to full 3D simulations (Figure 3), we primarily use 2D simulations to take advantage of reduced computation time to investigate numerous geometries as illustrative examples. The 3D structures corresponding to these 2D simulations are grating-like structures, which do not trap light as well as full 3D structures since only one incident polarization interacts strongly with the light trapping features. In this work, we consider unpolarized light, and thus we expect further absorption enhancements when 3D light trapping structures are fully optimized.

In conclusion, we have demonstrated the use of coupled optical and electrical modeling for the optimization of nanostructured solar cells. Detailed understanding of the physical mechanisms underlying performance allows for the advancement of this technique beyond simple design evaluation in order to guide optimization strategies. For n-i-p a-Si:H solar cells, we find that plasmonic and nanophotonic light trapping structures can be tailored to maximize absorption in the intrinsic region of the a-Si:H while mitigating parasitic absorption in the doped regions of the solar cell. We show that appropriately designed light trapping can have the same benefits as increasing absorber layer thickness and decreasing doped layer thicknesses, but avoid the drawbacks to performance, stability, processing, and cost concomitant with thicker devices. Of course most a-Si:H cells are made on randomly textured surfaces rather than flat layers. The improved control over light absorption achievable with controlled and designed nanostructures, in contrast, offers a method for directing light absorption to the optimal locations in the device. The principle of coupled optical and electrical design of light trapping in solar cells is broadly applicable other systems, including other thin-film materials and three dimensional geometries such as micro and nanowire devices,[20] and represents a powerful method for advanced device design in which optical design is used to simultaneously increase light absorption and optimize electrical device physics.

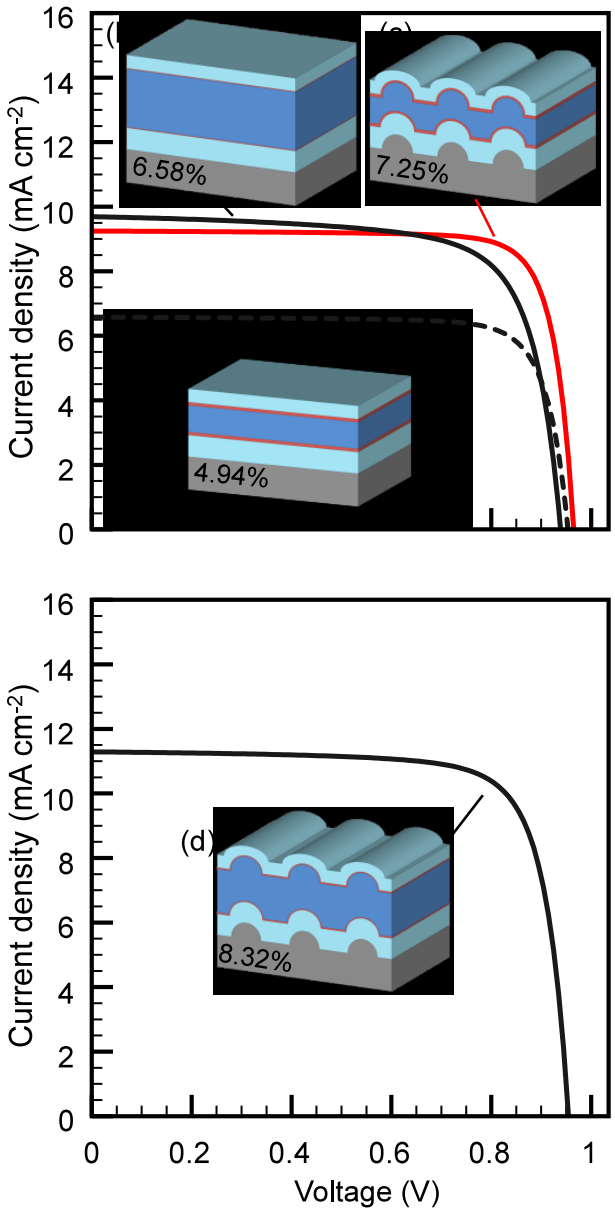

Figure 5. Current-voltage curves for solar cells with (a) a 200 nm thick a-Si:H layer with d = 20 nm, (b) a 360nm thick a-Si:H layer with d = 5 nm, (c) a conformal Ag cell with a 200 nm thick a-Si:H layer, d = 20 nm, and a feature pitch of 360 nm, and (d) the optimized geometry for the conformal Ag structure with a 290 nm thick a-Si:H layer, d = 10 nm, and pitch of 390 nm. The schematics are drawn to scale and correspond to the implied three-dimensional structures associated with the simulated plane. They have the same color scheme as in Figure 1, but with intrinsic a-Si:H indicated as dark blue and doped a-Si:H indicated as red. One-sun conversion efficiencies are indicated on the schematics. (b) is the design with the maximum efficiency we found for a flat cell without additional light trapping features for the material parameters used in this study; we note that it has degraded V_{oc} and FF compared to the other devices.

ASSOCIATED CONTENT

Supporting Information. Additional information and figures. This material is available free of charge via the Internet at http://pubs.acs.org.

AUTHOR INFORMAION

Corresponding Author

*haa@caltech.edu

ACKNOWLEDGMENT

We are grateful to Michael Kelzenberg, Daniel Turner-Evans, and Matthew Sheldon for useful discussions and assistance with the manuscript. This work was supported by the "Light-Material Interactions in Energy Conversion" Energy Frontiers Research Center, United States Department of Energy, under grant DE-SC0001293, LBL contract DE-AC02-05CH11231. One of us (MD) acknowledges support by the Office of Basic Energy Sciences under contract number DOE DE-FG02-07ER46405.

REFERENCES

1. Hall, R. N. *Solid-State Electronics* **1981,** 24, (7), 595-616.
2. Ferry, V. E.; Munday, J. N.; Atwater, H. A. *Adv Mater* **2010,** 22, (43), 4794-4808.
3. Green, M. A. *Electron Devices, IEEE Transactions on* **1984,** 31, (5), 671-678.
4. Ferry, V. E.; Verschuuren, M. A.; Li, H. B. T.; Verhagen, E.; Walters, R. J.; Schropp, R. E. I.; Atwater, H. A.; Polman, A. *Opt. Express* **2010,** 18, (S2), A237-A245.
5. Shah, A. V.; Schade, H.; Vanecek, M.; Meier, J.; Vallat-Sauvain, E.; Wyrsch, N.; Kroll, U.; Droz, C.; Bailat, J. *Progress in Photovoltaics: Research and Applications* **2004,** 12, (23), 113-142.
6. Atwater, H. A.; Polman, A. *Nat Mater* **2010,** 9, (3), 205-213.
7. Müller, J.; Rech, B.; Springer, J.; Vanecek, M. *Solar Energy* **2004,** 77, (6), 917-930.
8. Rockstuhl, C.; Fahr, S.; Bittkau, K.; Beckers, T.; Carius, R.; Haug, F. J.; Sˆderstrˆm, T.; Ballif, C.; Lederer, F. *Opt. Express* **2010,** 18, (S3), A335-A341.
9. Ferry, V. E.; Polman, A.; Atwater, H. A. *ACS Nano* **2011,** 5, (12), 10055-10064.

10. Ferry, V. E.; Verschuuren, M. A.; Lare, M. C. v.; Schropp, R. E. I.; Atwater, H. A.; Polman, A. *Nano Letters* **2011,** 11, (10), 4239-4245.
11. Zhu, J.; Hsu, C.-M.; Yu, Z.; Fan, S.; Cui, Y. *Nano Letters* **2010,** 10, (6), 1979-1984.
12. Pala, R. A.; White, J.; Barnard, E.; Liu, J.; Brongersma, M. L. *Advanced Materials* **2009,** 21, (34), 3504-3509.
13. Spinelli, P.; Hebbink, M.; de Waele, R.; Black, L.; Lenzmann, F.; Polman, A. *Nano Lett* **2011,** 11, (4), 1760-1765.
14. Bhattacharya, J.; Chakravarty, N.; Pattnaik, S.; Dennis Slafer, W.; Biswas, R.; Dalal, V. L. *Applied Physics Letters* **2011,** 99, (13), 131114.
15. Grandidier, J.; Callahan, D. M.; Munday, J. N.; Atwater, H. A. *Adv Mater* **2011,** 23, (10), 1272-1276.
16. Nagel, J. R.; Scarpulla, M. A. *Opt. Express* **2010,** 18, (S2), A139-A146.
17. Mallick, S. B.; Agrawal, M.; Peumans, P. *Opt. Express* **2010,** 18, (6), 5691-5706.
18. Mutitu, J. G.; Shi, S.; Chen, C.; Creazzo, T.; Barnett, A.; Honsberg, C.; Prather, D. W. *Opt. Express* **2008,** 16, (19), 15238-15248.
19. Battaglia, C.; Hsu, C.-M.; Söderström, K.; Escarré, J.; Haug, F.-J.; Charrière, M.; Boccard, M.; Despeisse, M.; Alexander, D. T. L.; Cantoni, M.; Cui, Y.; Ballif, C. *ACS Nano* **2012,** 6, (3), 2790-2797.
20. Kelzenberg, M. D.; Putnam, M. C.; Turner-Evans, D. B.; Lewis, N. S.; Atwater, H. A. In *Predicted efficiency of Si wire array solar cells*, Proceeding of the 34th IEEE PVSC, 2009; pp 001948-001953.
21. Li, X.; Hylton, N. P.; Giannini, V.; Lee, K.-H.; Ekins-Daukes, N. J.; Maier, S. A. *Opt. Express* **2011,** 19, (S4), A888-A896.
22. Heavens, O. S., *Optical properties of thin solid films*. General Publishing Company: Toronto, 1991.
23. Schiff, E. A. *Journal of Applied Physics* **2011,** 110, (10), 104501.
24. Yu, Z. F.; Raman, A.; Fan, S. H. *Proc. Natl. Acad. Sci. U. S. A.* **2010,** 107, (41), 17491-17496.
25. Beck, F. J.; Mokkapati, S.; Polman, A.; Catchpole, K. R. *Applied Physics Letters* **2010,** 96, (3), 033113.
26. Haug, F. J.; Söderström, T.; Cubero, O.; Terrazzoni-Daudrix, V.; Ballif, C. *Journal of Applied Physics* **2009,** 106, (4), 044502.
27. Schropp, R. E. I.; Zeman, M., *Amorphous and microcrystalline silicon solar cells: modeling, materials and device technology*. Kluwer Academic Publishers: Norwell, Massachusetts 1998.
28. Palik, E.; Ghosh, G., *Handbook of optical constants of solids*. Academic Press: New York, 1997; Vol. 3.
29. Rakic, A. D.; Djurišic, A. B.; Elazar, J. M.; Majewski, M. L. *Appl. Opt.* **1998,** 37, (22), 5271-5283.
30. *FDTD Solutions*, (http://www.lumerical.com).
31. *TCAD Sentaurus*, (http://www.synopsis.com).
32. Sze, S. M.; Ng, K. K., *Physics of semiconductor devices*. Wiley-Interscience: Hoboken, New Jersey, 2007.
33. Nelson, J., *The physics of solar cells*. Imperial College Press: London, 2003.
34. Swanson, R. M.; Beckwith, S. K.; Crane, R. A.; Eades, W. D.; Young Hoon, K.; Sinton, R. A.; Swirhun, S. E. *Electron Devices, IEEE Transactions on* **1984,** 31, (5), 661-664.
35. Kayes, B. M.; Atwater, H. A.; Lewis, N. S. *Journal of Applied Physics* **2005,** 97, (11), 114302.
36. Boettcher, S. W.; Spurgeon, J. M.; Putnam, M. C.; Warren, E. L.; Turner-Evans, D. B.; Kelzenberg, M. D.; Maiolo, J. R.; Atwater, H. A.; Lewis, N. S. *Science* **2010,** 327, (5962), 185-187.

37. Sakai, H.; Yoshida, T.; Hama, T.; Ichikawa, Y. *Japanese Journal of Applied Physics* **1990,** 29, 630-635.
38. Li, H. B. T.; Franken, R. H.; Rath, J. K.; Schropp, R. E. I. *Solar Energy Materials and Solar Cells* **2009,** 93, (3), 338-349.
39. Spinelli, P.; Verschuuren, M. A.; Polman, A. *Nature communications* **2012,** 3, 692.

TABLE OF CONTENTS IMAGE

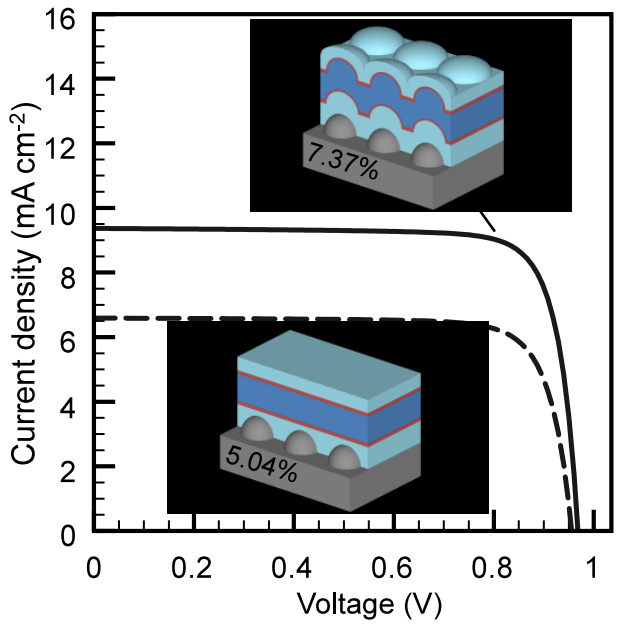

DISCLAIMER

This document was prepared as an account of work sponsored by the United States Government. While this document is believed to contain correct information, neither the United States Government nor any agency thereof, nor the Regents of the University of California, nor any of their employees, makes any warranty, express or implied, or assumes any legal responsibility for the accuracy, completeness, or usefulness of any information, apparatus, product, or process disclosed, or represents that its use would not infringe privately owned rights. Reference herein to any specific commercial product, process, or service by its trade name, trademark, manufacturer, or otherwise, does not necessarily constitute or imply its endorsement, recommendation, or favoring by the United States Government or any agency thereof, or the Regents of the University of California. The views and opinions of authors expressed herein do not necessarily state or reflect those of the United States Government or any agency thereof or the Regents of the University of California.

DE-AC02-05CH11231